Chemical Engineering Journal 271 (2015) 106–113

Contents lists available at ScienceDirect

Chemical Engineering Journal

journal homepage: www.elsevier.com/locate/cej

CO_2 chemisorption and evidence of the CO oxidation–chemisorption mechanisms on sodium cobaltate

Elizabeth Vera, Brenda Alcántar-Vázquez, Heriberto Pfeiffer *

Instituto de Investigaciones en Materiales, Universidad Nacional Autónoma de México, Circuito exterior s/n, Cd. Universitaria, Del. Coyoacán C.P. 04510, México DF, Mexico

HIGHLIGHTS

- Sodium cobaltate is able to chemisorb CO_2 in a wide temperature range.
- Sodium cobaltate was evaluated as CO oxidant catalyst.
- CO oxidation–chemisorption double reaction mechanism was studied.

GRAPHICAL ABSTRACT

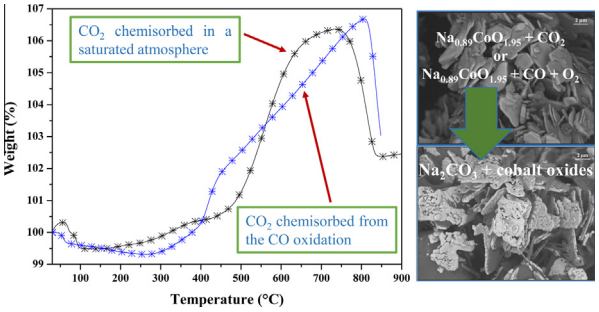

ARTICLE INFO

Article history:
Received 19 December 2014
Received in revised form 18 February 2015
Accepted 19 February 2015
Available online 26 February 2015

Keywords:
CO oxidation
CO_2 chemisorption
Sodium cobaltate
Thermal analysis

ABSTRACT

Sodium cobaltate was synthesized, characterized (structural and microstructural) and evaluated for CO_2 and CO captures. The CO capture was produced via a double reaction mechanism oxidation–chemisorption process. The sample structure and composition were studied using the XRD and atomic absorption techniques, which indicated a $Na_{0.89}CoO_{1.95}$ composition. This ceramic is able to chemically trap CO_2, which results in carbonation products such as Na_2CO_3 and different cobalt oxides. Cobalt was chemically reduced as a function of the carbonation temperature. The $Na_{0.89}CoO_{1.95}$–CO_2 reaction kinetic parameters were determined assuming a first-order reaction. The kinetic constants tend to increase as a function of temperature, and two different $\Delta H^{\ddagger}$ values were determined. On the other hand, the $Na_{0.89}CoO_{1.95}$–CO oxidation and subsequent chemisorption processes were analyzed. CO can be oxidized on sodium cobaltate and chemically trapped above 160 °C (total conversion was obtained at 490 °C).

1. Introduction

Since the industrial revolution, fossil fuels, such as coal, petroleum and natural gas, remain important energy sources. Therefore, the concentration of atmospheric CO_2 has gradually increased. The emissions of CO_2, which is a major greenhouse gas, need to be reduced. For this purpose, innovative technologies for carbon capture and storage have been developed in recent years. In addition, methane autothermal reforming with CO_2 and oxygen, which is a combination of CO_2 reforming and partial oxidation reactions, has drawn significant interest in recent years as alternative routes for conversion of natural gas to syngas, which is a mixture of CO and H_2 that can be used to obtain products with high added values, such as ammonia, hydrocarbons and oxygenated compounds [1]. In addition, increasing demands for clean fuel has directed attention to fuel cell systems based on hydrogen fuel that are highly efficient with fewer air pollutants [2].

In the field of CO_2 capture, several alkaline ceramics have been proposed as possible CO_2 chemisorbents [3–6]. Within these alkaline ceramics, Li_2ZrO_3, Li_4SiO_4, Li_2CuO_2 and Na_2ZrO_3, among others, have been extensively studied, because they exhibit good CO_2

* Corresponding author. Tel.: +52 (55) 5622 4627; fax: +52 (55) 5616 1371.
E-mail address: pfeiffer@iim.unam.mx (H. Pfeiffer).

http://dx.doi.org/10.1016/j.cej.2015.02.075
1385-8947/

capture properties. For example, CO_2 chemisorption temperature range, good cyclability and good kinetic properties [7–24].

In addition, the use of these materials may be linked to CO_2 capture and subsequent conversion to different added value products. [25–30] For example, in steam reforming (SR), the H_2/CO ratio can be varied by manipulating the relative concentrations of CO_2 and O_2 in the feed, which can be achieved via selectively adsorbing the co-generated CO_2 on a proper and effective sorbent and/or by carbon monoxide oxidation [31]. A typical sorbent has specific characteristics, including (i) selective sorption of CO_2 at the process temperature and in presence of steam, CH_4, CO, and H_2, (ii) adequate working CO_2 capacity at the process operational temperature, (iii) adequate rates of sorption and desorption, and (iv) adequate thermal and cyclic stability under the process conditions. High purity H_2 (>95%) and the reduction of CO in the gas effluent to ppm levels are the most important advantages [26,27].

Therefore, various methods have been proposed for CO removal, such as selective diffusion, pressure swing adsorption, selective CO oxidation, and CO methanation [32]. However, the catalytic oxidation of CO in H_2-rich gas is considered a promising method and the most cost-effective approach for eliminating CO from reformed fuels. An efficient catalyst must exhibit certain characteristics including (i) high CO conversion and oxidation rate at a wide operating temperature range, (ii) high selectivity for CO oxidation reaction with respect to undesired H_2 oxidation, and (iii) stability within the time on stream [32]. Noble and transition metals (i.e., Pt, Pd, Au, Ru, Co, Cu) have been widely studied as catalysts. In general, these materials require a support, such as zeolites and Al_2O_3, which complicates their preparation and increases the cost. In addition, the catalytic activity is reduced by contamination due to carbon deposition on the catalyst surface [31,33–36].

However, Na_xCoO_2 compounds are layered oxide materials that are used in thermoelectric applications. These compounds have received much attention because they are nonpoisonous and due to their lower cost, simple synthesis and anti-oxidization, which occurs in an oxidized atmosphere for a long time [37–42]. The crystal structure of Na_xCoO_2 consists of hexagonal CoO_2 blocks and a Na layer that form a layered structure. The Na layer is highly vacant, and the crystal structure varies with the Na content [43–45].

Similar alkaline ceramics, with layered structures, have been analyzed as possible CO_2 captors, showing interesting results. In these cases, the alkaline element can diffuse easily, improving the CO_2 chemisorption process [18–21,24]. In addition, it has been probed that the formation of different structural defects on the alkaline ceramics modified the diffusion processes [10,20–12,24,48]. Therefore, the crystalline structure of this material might improve the sodium diffusion in the CO_2 chemisorption process. Additionally, the cobalt content may induce a catalytic activity in the CO oxidation reaction. None of these possible sodium cobaltate applications have been previously reported. Therefore, in the current work, sodium cobaltate was studied for use in CO_2 capture and as a CO oxidation catalyst (including a subsequent CO_2 capture) under different temperature conditions.

2. Experimental section

Na_xCoO_2 was synthesized using a solid-state reaction with sodium carbonate (Na_2CO_3, Aldrich) and cobalt carbonate hydrate ($CoCO_3{\cdot}xH_2O$, Aldrich). A 27 wt% excess of sodium carbonate was used to obtain $NaCoO_2$, due to the sodium tendency to sublimate [18–20]. The powders were mechanically mixed and thermally treated at 850 °C for 12 h. A diffractometer (Siemens, D5000) with a Co-Kα (1.7903 Å) radiation source operating at 34 kV and 30 mA was used to identify the pristine phase and the products after CO_2 analyses. The samples were measured in a 2-theta range of 15–70° with a step size of 0.016°. The phases were identified using the Joint Committee Powder Diffraction Standards (JCPDS). The microstructure was analyzed using scanning electron microscopy (SEM). The SEM analysis was performed on a JEOL JMS-7600F.

To determine the concentration of sodium and cobalt in the sample, atomic absorption was performed (Varian Spectra, AA220). Prior to the analysis, the sample was dissolved in a HNO_3 concentrated solution (68–70%, Sigma-Aldrich) using a microwave system (CEM, MDS 2000). The calibration was performed with the standard high-purity standard QCS 26. The nitrogen adsorption–desorption isotherm of the Na_xCoO_2 sample was obtained on a Bel-Japan Minisorp II instrument at 77 K using a multipoint technique (N_2 from Praxair, grade 4.8). Prior to analysis, the sample was degassed at room temperature for 67 h. The surface area was determined using the Brunauer–Emmett–Teller (BET) method.

Dynamic and isothermal CO_2 capture analyses were performed with a Q500HR instrument (TA Instruments). Initially, the sample was dynamically heated from 30 to 900 °C at a heating rate of 5 °C/min using a CO_2 flow rate of 60 mL/min (Praxair, grade 3.0). Then, the Na_xCoO_2 sample was isothermally analyzed in the same CO_2 flux at different temperatures (from 400 to 765 °C). For the isothermal analysis, the samples were heated to the desired temperature under a N_2 flux (Praxair, grade 4.8). Once the corresponding temperature was reached, the flow gas was switched from N_2 to CO_2. After the CO_2 capture process, the structural and microstructural evolution of the Na_xCoO_2 sample was analyzed using X-ray diffraction (XRD) and SEM.

For the CO oxidation–chemisorption analysis, a thermogravimetric analysis was performed using a Q500HR instrument (TA Instruments). Initially, the sample was dynamically heated from 30 to 850 °C at a heating rate of 5 °C/min using a gas mixture of 5 vol% O_2 (Praxair, grade 2.6) and 5 vol% CO and N_2 (Praxair, certificate standard) as a balance and carrier gas with a total flow rate of 60 mL/min. In addition, the CO oxidation was evaluated in a Bel-Rea catalytic reactor (Bel Japan) using the same gas mixture described above using a total flow rate of 100 sccm with 200 mg of catalyst. Initially, the sample was cleaned under a 50 sccm N_2 flow for 15 min. Then, the sample was dynamically heated from 30 to 900 °C at a heating rate of 5 °C/min. The gas products were analyzed with a GC 2014 gas chromatograph (Shimadzu) with a Carboxen-100 column and an Alpha Platinum FTIR spectrometer (Bruker) connected to a ZnS gas flow cell.

3. Results and discussion

Sodium cobaltate was synthesized using a solid-state reaction. Fig. 1 shows the XRD pattern, which was fitted to 01-087-0274 PDF, corresponding to the $Na_{0.74}CoO_2$ phase even though the nominal formula was $NaCoO_2$. This result was confirmed by elemental analysis, and the experimental formula was determined to be $Na_{0.89}CoO_{1.95}$. Because a non-stoichiometric formula was obtained ($Na_{0.89}CoO_{1.95}$), some cationic and anionic vacancies may be present in the Na_xCoO_2 structure, as it has been previously described [43–45]. Equation (1) represents the different kind of vacancies. Therefore, these vacancies might improve the sodium diffusion through the structure during CO_2 chemisorption and CO oxidation–chemisorption, as it has been reported for other alkaline ceramics ($Na_2(Zr–Al)O_3$, $Li_{2+x}CuO_{2+x/2}$ and $Li_4(Si–Al)O_4$, among others [10,20–21,24,48]).

$$Na_{Na} + Co_{Co} + 2O_O \rightarrow 0.89Na_{Na} + Co_{Co} + 1.95O_O + 0.11V'_{Na} + 0.05V_o^{\cdot\cdot} \quad (1)$$

After the structural and compositional identification, the microstructural characteristics of the sample were analyzed by

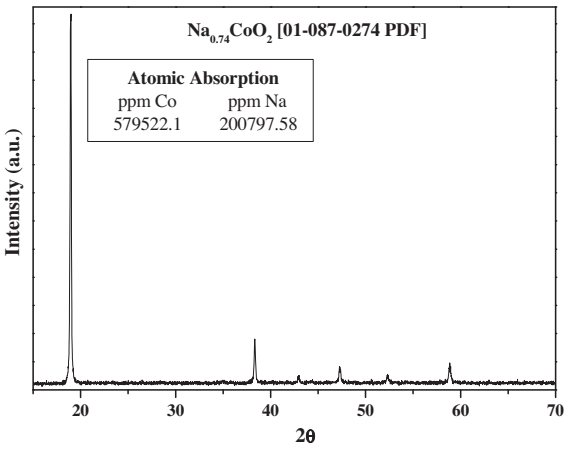

Fig. 1. XRD pattern for the pristine $Na_{0.89}CoO_{1.95}$ sample.

SEM and N_2 adsorption-desorption (Fig. 2). The backscattered electron images of the sodium cobaltate show some of its morphological characteristics. The $Na_{0.89}CoO_{1.95}$ sample formed well-defined polyhedral flake-like particles that varied in size from 1 to 5 μm with a thickness of 50–200 nm. These flake-like particles appear to produce non-dense agglomerates that are approximately 10–20 μm. Therefore, to complete the microstructural characterization of $Na_{0.89}CoO_{1.95}$, the sample was analyzed using N_2 adsorption-desorption (see Fig. 2 inset). The N_2 adsorption–desorption curve corresponds to a type II isotherm according to the IUPAC classification [46], and the isotherm did not exhibit hysteresis. This behavior corresponds to non-porous particles. The sample surface area was estimated to be 2.0 m^2/g using the BET model [46].

The combination of sodium and cobalt in the sodium cobaltate may induce the presence of different physicochemical effects or reactions with carbon oxides, such as CO oxidation and/or CO_2 capture. These processes may be of great interest for the design of separation systems from different flow gas effluents. Therefore, it is very important to understand the CO_2 capture properties of this ceramic even though the Na/Co molar ratio is not as high as that in other alkaline ceramics [7–24,47]. Based on this perspective, CO_2 chemisorption on sodium cobaltate was studied.

According to previous studies, based on sodium and lithium ceramics, a general reaction between $NaCoO_2$ and CO_2 would be expected to follow reaction (2):

$$2NaCoO_2 + CO_2 \rightarrow Na_2CO_3 + Co_2O_3 \quad (2)$$

Fig. 3 shows the $Na_{0.89}CoO_{1.95}$ dynamic thermogram in a CO_2 flow. Initially, the sample exhibited a small weight decrease (1 wt%), which was associated with a superficial dehydration process. Next, the thermogram indicated a continuous weight gain between 150 and 740 °C. In fact, this weight can be divided into two clear temperature ranges from 180 to 415 °C and 415 to 740 °C, corresponding to the superficial and bulk CO_2 chemisorption processes, respectively. This result is in agreement with other sodium and lithium ceramics where their respective dynamic thermograms exhibit one or two consecutive weight increments associated with the superficial and bulk CO_2 chemisorption processes followed by a final weight decrease associated with CO_2 desorption [7,11,15,17–24]. In this sample, the first maximum weight increase, which was equal to 0.8 wt%, was observed at ~400 °C. Then, between 415 and 740 °C, the thermogram indicated a second total weight increase of 6.8 wt%. After this weight increase, the weight began to decrease due to the decarbonation process.

As expected, the final weight increase was not as high as that observed in other ceramics due to the Na/Co molar ratio, which was low. Nevertheless, the dynamic thermogram reached a final efficiency equal to 38.4%, which is comparable to that of other sodium and lithium ceramics with higher alkaline/metal molar ratios [10,14,16–18,20,21,47]. Therefore, different isothermal experiments were performed, and the products obtained from those isotherms were re-characterized by XRD and SEM to confirm CO_2 chemisorption and elucidate the possible reaction mechanism.

Fig. 4 shows the $Na_{0.89}CoO_{1.95}$ isotherms obtained at different temperatures in a CO_2 flow. The initial isothermal experiment was performed at 400 °C. This isotherm exhibited an exponential behavior and did not reach equilibrium after 3 h, and the weight increase was only 2.4 wt%. The subsequent isotherms were performed between 400 and 700 °C at 50 °C increments. All of these isotherms exhibited typical exponential behavior where the weight gained increased as a function of temperature from 4.7 wt% at 450 °C to 9.9 wt% at 700 °C, which corresponded to the maximum weight increase. In fact, at this temperature, the CO_2 chemisorption equilibrium was reached after two hours, which represents a final efficiency of 55.9%. At higher temperatures (725, 750 and 765 °C), the isotherms indicated partial desorption

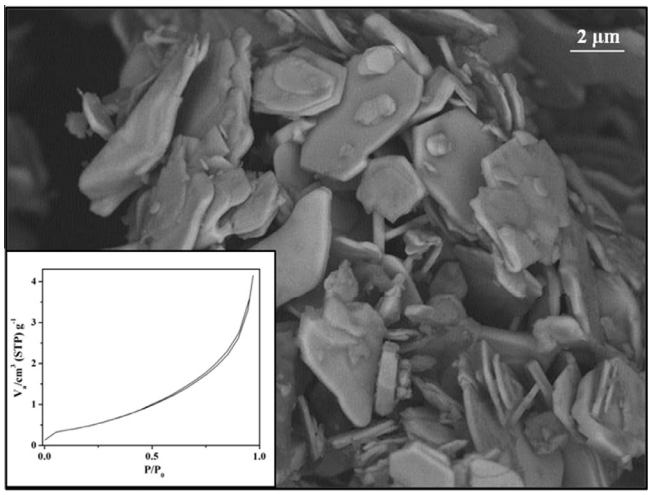

Fig. 2. Scanning electron image of the $Na_{0.89}CoO_{1.95}$ pristine sample and N_2 adsorption–desorption isotherm (square inset).

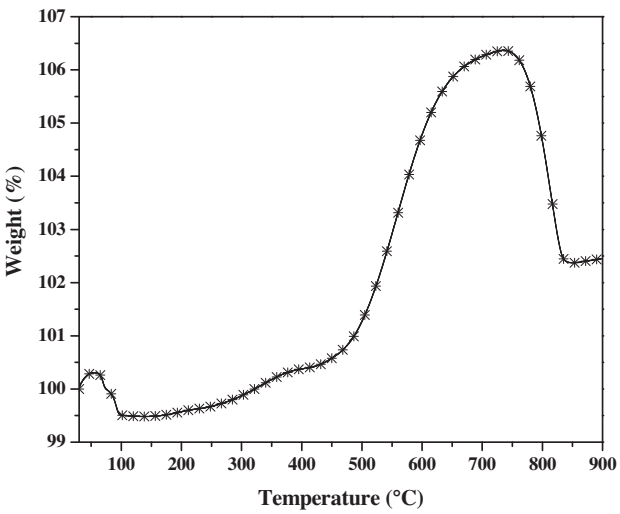

Fig. 3. $Na_{0.89}CoO_{1.95}$ dynamic thermogram in a CO_2 flow.

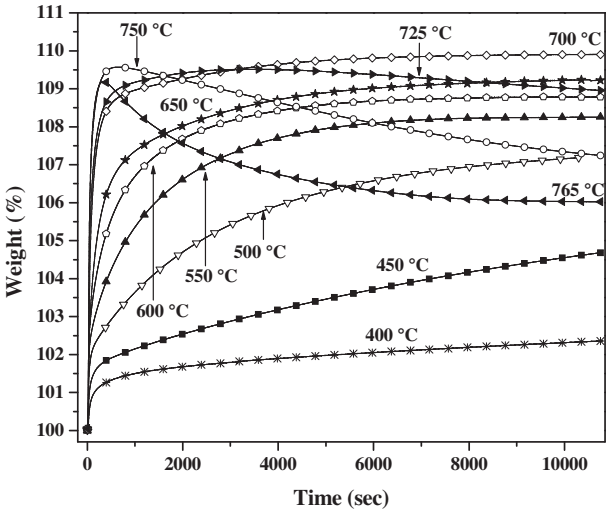

Fig. 4. CO_2 chemisorption isothermal analysis of $Na_{0.89}CoO_{1.95}$ at different temperatures.

even though these isotherms exhibited important weight increases (~9 wt%) during the first few minutes. These results indicated that the CO_2 chemisorption-desorption equilibrium was modified in this temperature range.

To understand the CO_2–$Na_{0.89}CoO_{1.95}$ chemisorption mechanism, the isothermal products were analyzed by XRD and SEM. Fig. 5 shows the XRD patterns of different CO_2–$Na_{0.89}CoO_{1.95}$ isothermal products. The initial $Na_{0.89}CoO_{1.95}$ diffraction pattern was included for comparison purposes. The 400 °C sample product consisted of the formation of Co_3O_4, and the crystallinity of $Na_{0.89}CoO_{1.95}$ appeared to be destroyed. In addition, from this XRD pattern, the (002) peak was shifted to the left compared to that in XRD pattern of the $Na_{0.89}CoO_{1.95}$ pristine sample. Therefore, the $Na_{0.89}CoO_{1.95}$ structure and crystallinity were modified, which may be due to a partial sodium release that was observed in the corresponding thermogravimetric experiments. At higher temperatures (450–700 °C), all of the XRD patterns and crystalline phases exhibit the following trend. While the $Na_{0.89}CoO_{1.95}$ phase tended to disappear, Na_2CO_3 appeared, and Co_3O_4 increased. However, CoO was produced instead of Co_3O_4 at $T > 700$ °C. As expected, the appearance of Na_2CO_3 was due to

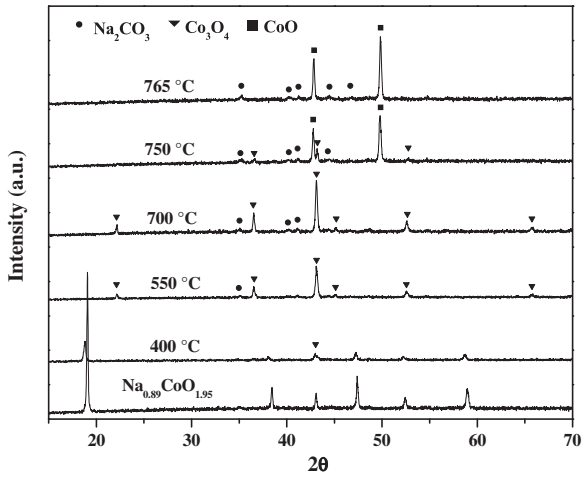

Fig. 5. XRD patterns of different CO_2–$Na_{0.89}CoO_{1.95}$ isothermal products.

CO_2 chemisorption. However, in reaction (2), a different cobalt oxide (Co_2O_3) has been proposed based on cobalt not changing its valence (+3). However, the results clearly show that the valence of cobalt changes from +3 to +2 because the cobalt oxides detected by XRD were Co_3O_4 and CoO. In other words, cobalt was reduced as a function of temperature. Therefore, some oxygen must be consecutively released, as shown in reactions (3) and (4). In fact, the oxygen release was confirmed by gas chromatography (data not shown).

$$3Co_2O_3 \xrightarrow{400-700\ ^\circ C} 2Co_3O_4 + 1/2\ O_2 \quad (3)$$

$$Co_3O_4 \xrightarrow{T>700\ ^\circ C} 3CoO + 1/2\ O_2 \quad (4)$$

To complement the isothermal product analysis, SEM images were obtained. Fig. 6 shows different morphological aspects of the CO_2–$Na_{0.89}CoO_{1.95}$ products obtained at 550 and 700 °C. The morphology of the samples did not appear to result in important variations compared to the original $Na_{0.89}CoO_{1.95}$ sample (see Fig. 2). The particles exhibited the same flake-like particle morphology, and the sizes did not change. However, the backscattered images clearly indicated the presence of two different phases. The presence of these phases was determined by the particle contrasts observed in the corresponding back scattered electron images (BSEI), and these phases must correspond to Na_2CO_3 and cobalt oxide because they were the $Na_{0.89}CoO_{1.95}$ carbonation products

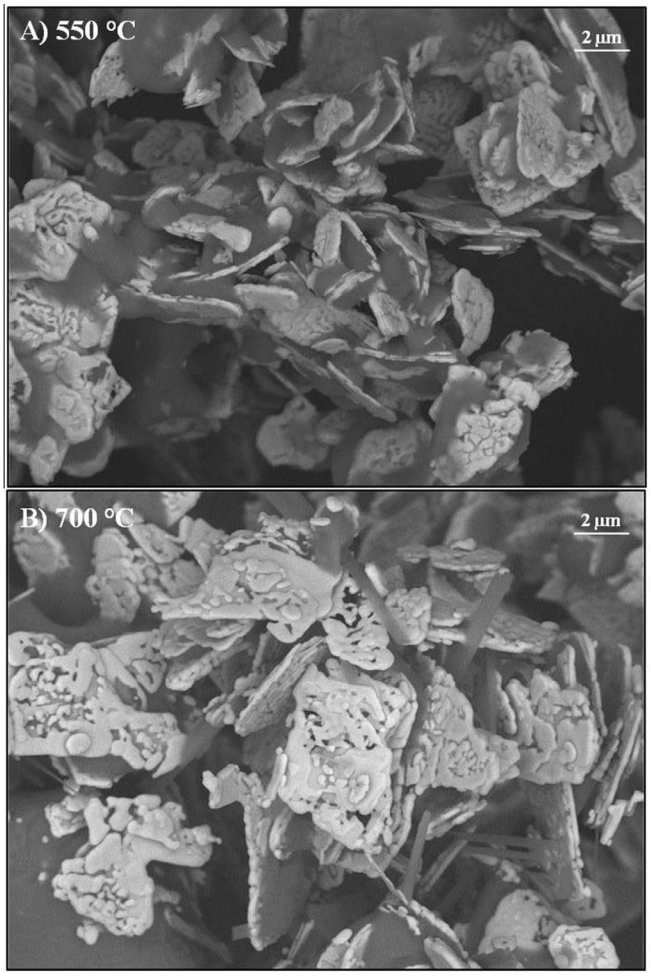

Fig. 6. Scanning electron images of the isothermal products obtained at 550 and 700 °C.

detected by XRD. Therefore, the contrast differences arise from the differences in the mean atomic number ($\bar{z}$) (the $\bar{z}$ values for Na_2CO_3, Co_3O_4 and CoO are 8.666, 16.142 and 17.5, respectively). Therefore, the backscattered electron coefficient (η) of these phases increases from 0.0998 for Na_2CO_3 (dark phase) to 0.1879 (Co_3O_4) or 0.2021 (CoO) for any of the cobalt oxides (light phase). Finally, it must be noted that at 700 °C, some filaments, which consist of Na_2CO_3, were detected.

To further analyze the isothermal curves shown in Fig. 4, these data were fitted to a first-order reaction [14,18,49]. This model was selected because there are several processes involved in this reaction mechanism, such as different CO_2 chemisorption processes (superficial and bulk chemisorptions) and cobalt reduction processes. Therefore, the data could not be fitted to multiple exponential models. However, during the first moments of the CO_2 chemisorption process, one can assume that a first-order reaction occurred with respect to $Na_{0.89}CoO_{1.95}$ surface particles because CO_2 was present in excess (60 mL/min). Therefore, the rate law can be assumed to be:

$$\ln[Na_{0.89}CoO_{1.95}] = -kt \quad (5)$$

where k is the reaction rate constant, t is the time, and $[Na_{0.89}CoO_{1.95}]$ is the molar concentration of the ceramic. Assuming a superficial $Na_{0.89}CoO_{1.95}$ carbonation reaction, the data trends were linear only over very short intervals (20 s approximately) before any diffusion processes, structural changes or cobalt reduction occur. Table 1 shows the k values obtained, which tend to increase in two different temperature ranges between 400 and 600 °C and between 650 and 750 °C. This trend was confirmed when the k values were plotted according to Eyring's model, which is used for heterogeneous reactions (Fig. 7). With this model, two different activation enthalpy values ($\Delta H^{\ddagger}$) were determined. Between 400 and 600 °C, the $\Delta H^{\ddagger}$ value was 48.8 kJ/mol, and at $T > 600$ °C, the $\Delta H^{\ddagger}$ value was equal to 52.8 kJ/mol. The $\Delta H^{\ddagger}$ change may be related to different factors, such as the CO_2 chemisorption–desorption equilibrium, intercrystalline diffusion processes and cobalt reduction.

In addition, these k and $\Delta H^{\ddagger}$ values are not substantially different from those reported for other sodium ceramics [18,20,47,48]. For example, the reported k values for Na_2ZrO_3 are between 1×10^{-3} and 2×10^{-2} s^{-1} at the optimum CO_2 capture temperatures (i.e., 600–700 °C) with a $\Delta H^{\ddagger}$ value of 33 kJ/mol [18,20], and Na_2TiO_3 exhibited a k values of 1.7–2.5 $\times 10^{-4}$ s^{-1} and a $\Delta H^{\ddagger}$ value of 140.9 kJ/mol under the best capture conditions (i.e., 600 and 650 °C) [49]. Therefore, these results clearly indicate that CO_2 chemisorption on $Na_{0.89}CoO_{1.95}$ was slower than that on Na_2ZrO_3 but considerably faster than that on Na_2TiO_3. These differences may be related to CO_2 chemisorption evolution present in these sodium ceramics. Na_2ZrO_3 and $Na_{0.89}CoO_{1.95}$ evolve directly to Na_2CO_3 and the corresponding metal oxides and their $\Delta H^{\ddagger}$ values does not change so much in the corresponding temperature range. On the other hand, Na_2TiO_3 only reacts partially with CO_2 producing Na_2CO_3 and different sodium titanates with lower Na:Ti molar ratios. In addition, these sodium titanate secondary phases are denser, which reduces the diffusion processes according to the k values obtained in each case.

Table 1
k values obtained from the first order reaction model.

T (°C)	k (1/s)	R^2
400	5.33×10^{-4}	0.9985
450	1.28×10^{-3}	0.9985
500	2.65×10^{-3}	0.9988
550	3.49×10^{-3}	0.9969
600	5.22×10^{-3}	0.9971
650	3.10×10^{-3}	0.9990
700	3.43×10^{-3}	0.9903
725	5.65×10^{-3}	0.9980
750	6.49×10^{-3}	0.9982
765	5.77×10^{-3}	0.9964

After the CO_2 chemisorption analyses, CO oxidation and the consecutive chemisorption on sodium cobaltate was explored. These processes were evaluated by thermogravimetric and gas chromatography analyses. Fig. 8 shows the thermogram obtained in a $CO–O_2$ flow compared with the sample analyzed under a CO_2 flow. Both thermograms exhibited similar behaviors even though the samples were analyzed under different conditions. While the $CO–O_2$ experiment was performed with a diluted gas flow (N_2:CO = 95:5), the CO_2 experiment was obtained from a CO_2 saturated flow. In both cases, the total flow was equal to 60 mL/min. The superficial capture process was observed between 280 and 400 °C in a $CO–O_2$ flow, and the bulk chemisorption process was observed between 400 and 805 °C. From these thermograms, both processes (superficial and bulk) were shifted to higher temperatures in a $CO–O_2$ flow compared to the processes observed in CO_2. The thermal shifts may be due to the double and consecutive processes produced in the CO oxidation–chemisorption experiment where both processes were produced by $Na_{0.89}CoO_{1.95}$.

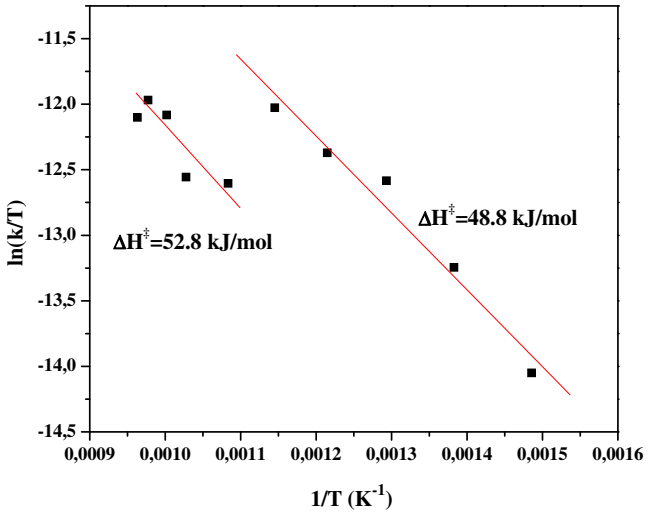

Fig. 7. Eyring-type plot of ln k/T as a function of $1/T$ for data obtained assuming a first-order reaction of $[Na_{0.89}CoO_{1.95}]$.

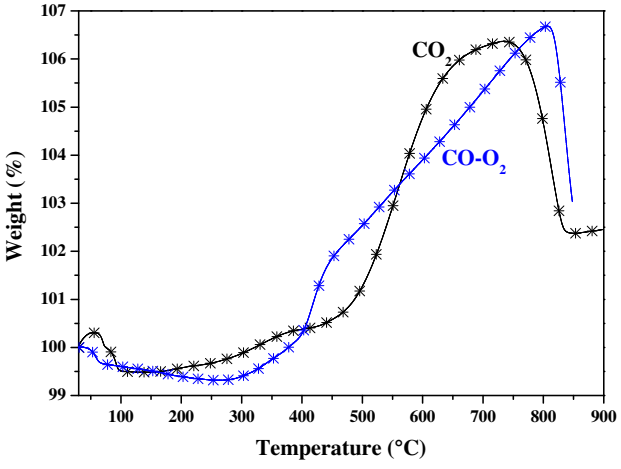

Fig. 8. Dynamic thermograms of $Na_{0.89}CoO_{1.95}$ in $CO–O_2$ (diluted in 90% of N_2) and saturated CO_2 flows. The total gas flux was 60 mL/min in both cases.

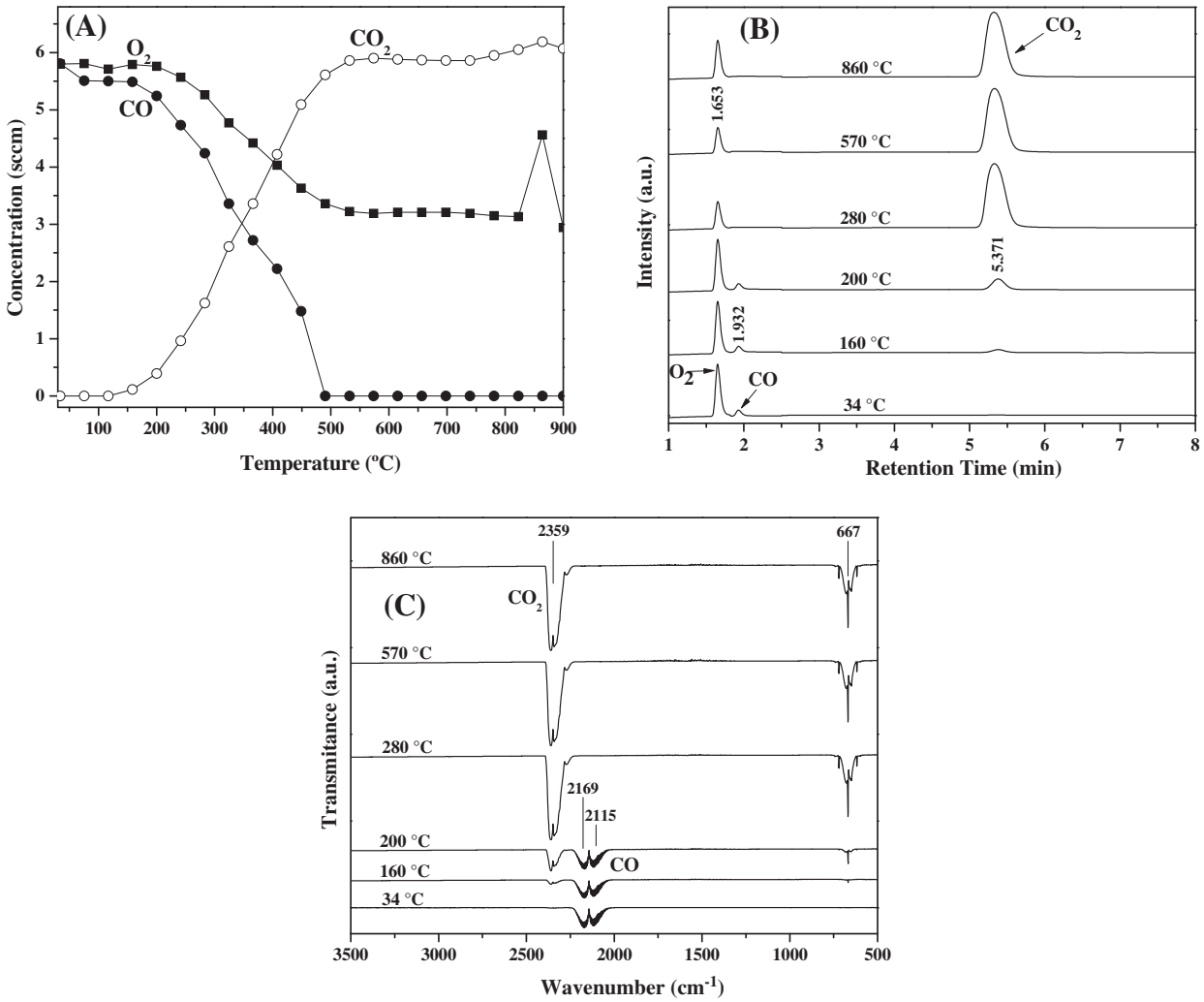

Fig. 9. Dynamic thermal CO, O_2 and CO_2 evolution using $Na_{0.89}CoO_{1.95}$ as a catalyst (A), gas chromatograms (B) and FTIR spectra (C) obtained from the gas products at different temperatures.

From this thermogram comparison, it must be noted that the slopes of the weight increases of the CO–O_2 and CO_2 bulk chemisorption processes are significantly different; 0.0138 and 0.0287 wt%/°C, respectively. These slope values strongly suggest that the CO–O_2 chemisorption kinetics were slower than those of CO_2.

To confirm the CO oxidation and subsequent chemisorption, which was assumed based on the weight increases observed in the previous thermogram, CO oxidation was dynamically evaluated in a catalytic reactor connected to a gas chromatograph and a FTIR gas cell (Fig. 9). CO catalytic transformation and subsequent CO_2 production were observed at very low temperatures. Between room temperature and 120 °C, CO and O_2 did not appear to vary. In other words, the catalytic reaction did not occur. Nevertheless, CO_2 was observed at approximately 160 °C, and total conversion was achieved at 490 °C. The CO and O_2 composition did not vary from 490 °C to 860 °C. However, at 860 °C, the O_2 concentration increased. This O_2 increase is in good agreement with the Co valence change mentioned above. In addition, the CO_2 concentration appeared to increase at temperatures higher than 830 °C. This increase must be related to the Na_2CO_3 decomposition process, which was produced during CO_2 chemisorption (previously detected by thermogravimetric analyses).

The total CO oxidation process is in very good agreement with the initial weight increase associated with CO_2 superficial chemisorption (see Fig. 8). Therefore, all of these results confirm that CO oxidation–chemisorption occurred in the $Na_{0.89}CoO_{1.95}$ particles via a double reaction process at $T \geqslant 160$ °C:

$$CO + 1/2\ O_2 \xrightarrow{Na_{0.89}CoO_{1.95}} CO_2 \quad (6)$$

$$Na_{0.89}CoO_{1.95} + \frac{0.89}{2}CO_2 \longrightarrow \frac{0.89}{2}Na_2CO_3 + \text{cobalt oxides} \quad (7)$$

In reaction (7), the cobalt oxide composition depends on temperature, as previously discussed. In addition, it must be pointed out that the CO oxidation is produced independently of the $Na_{0.89}CoO_{1.95}$ carbonation degree.

4. Conclusions

Sodium cobaltate was synthesized via a solid-state reaction. The sample structure, composition ($Na_{0.89}CoO_{1.95}$) and microstructure were analyzed using XRD, ICP, SEM and N_2 adsorption. The CO_2 chemisorption and CO oxidation–chemisorption capacities on $Na_{0.89}CoO_{1.95}$ were evaluated. The CO_2 chemisorption process was dynamically and isothermally analyzed using thermogravimetric analyses. Then, the carbonation products were re-characterized using XRD and SEM. Between 150 and 740 °C, CO_2 is chemisorbed on $Na_{0.89}CoO_{1.95}$, which resulted in the production

of Na_2CO_3 and different cobalt oxides depending on the temperature range (determined by XRD). In fact, cobalt was reduced as a function of the carbonation temperature. The kinetic parameter values (k) obtained for the $Na_{0.89}CoO_{1.95}$–CO_2 reaction mechanism tends to increase as a function of temperature. In addition, two different $\Delta H^{\ddagger}$ values were determined; 48.8 and 52.8 kJ/mol at 400–600 °C and T > 600 °C, respectively. Therefore, CO_2 chemisorption on $Na_{0.89}CoO_{1.95}$ may be related to a variety of factors, such as the CO_2 chemisorption–desorption equilibrium, intercrystalline diffusion processes and cobalt reduction.

Additionally, the CO oxidation–chemisorption processes on $Na_{0.89}CoO_{1.95}$ were studied. The analysis was performed using a catalytic reactor connected to a gas chromatograph and FTIR spectrometer with a thermobalance. The results confirmed that CO was oxidized and chemically trapped on sodium cobaltate at different temperatures. CO oxidation was observed at 160 °C, and total conversion was achieved at 490 °C. The results of the thermogravimetric experiments indicated that CO is chemically trapped after the oxidation process on $Na_{0.89}CoO_{1.95}$.

Acknowledgments

This work was financially supported by the SENER-CONACYT 150358 and PAPIIT-UNAM IN-102313 projects. Elizabeth Vera wishes to thank CONACYT for financial support. We wish to thank Adriana Tejeda and Omar Novelo for technical assistance.

References

[1] J. Gao, J. Guo, D. Liang, Z. Hou, J. Fei, X. Zheng, Production of syngas via autothermal reforming of methane in a fluidized-bed reactor over the combined CeO_2–ZrO_2/SiO_2 supported Ni catalysts, Int. J. Hydrogen Energy 33 (2008) 5493–5500.
[2] B. Nematollahi, M. Rezaei, M. Khajenoori, Combined dry reforming and partial oxidation of methane to synthesis gas on noble metal catalysts, Int. J. Hydrogen Energy 36 (2011) 2969–2978.
[3] S. Kumar, S.K. Saxena, A comparative study of CO_2 sorption properties for different oxides, Mater. Renew. Sustain. Energy 3 (2014) 1–15.
[4] J. Wang, L. Huang, R. Yang, Z. Zhang, J. Wu, Y. Gao, Q. Wang, D. O'Hare, Z. Zhong, Recent advances in solid sorbents for CO_2 capture and new development trends, Energy Environ. Sci. 7 (2014) 3478–3518.
[5] S. Choi, J. Drese, C. Jones, Adsorbent materials for carbon dioxide capture from large anthropogenic point sources, ChemSusChem 2 (2009) 796–854.
[6] B. Nair, R. Burwood, V. Goh, K. Nakagawa, T. Yamaguchi, Lithium based ceramic materials and membranes for high temperature CO_2 separation, Prog. Mater. Sci. 54 (2009) 511–541.
[7] A. Iwana, H. Stephensonb, W.C. Ketchiec, A.A. Lapkin, High temperature sequestration of CO_2 using lithium zirconates, Chem. Eng. J. 146 (2009) 249–258.
[8] M.B.I. Chowdhury, M.R. Quddus, H.I. deLasa, CO_2 capture with a novel solid fluidizable sorbent: thermodynamics and temperature programmed carbonation–decarbonation, Chem. Eng. J. 232 (2013) 139–148.
[9] M.R. Quddus, M.B.I. Chowdhury, H.I. deLasa, Non-isothermal kinetic study of CO_2 sorption and desorption using a fluidizable Li_4SiO_4, Chem. Eng. J. 15 (2015) 347–356.
[10] J. Ortiz-Landeros, T.L. Ávalos-Rendon, C. Gómez-Yáñez, H. Pfeiffer, Analysis and perspectives concerning CO_2 chemisorption on lithium ceramics using thermal analysis, J. Therm. Anal. Calorim. 108 (2012) 647–655.
[11] S. Wang, C. An, Q.H. Zhang, Syntheses and structures of lithium zirconates for high-temperature CO_2 absorption, J. Mater. Chem. A 1 (2013) 3540–3550.
[12] R. Rodríguez-Mosqueda, H. Pfeiffer, Thermokinetic analysis of the CO_2 chemisorption on Li_4SiO_4 by using different gas flow rates and particle sizes, J. Phys. Chem. A 114 (2010) 4535–4541.
[13] S.Y. Shan, Q.M. Jia, L.H. Jiang, Q.C. Li, Y.M. Wang, J.H. Peng, Novel Li_4SiO_4-based sorbents from diatomite for high temperature CO_2 Capture, Ceram. Int. 39 (2013) 5437–5441.
[14] Z. Qi, H. Daying, L. Yang, Y. Qian, Z. Zibin, Analysis of CO_2 sorption/desorption kinetic behaviors and reaction mechanism on Li_4SiO_4, AIChE J. 59 (2013) 901–911.
[15] Q. Xiao, X. Tang, Y. Liu, Y. Zhong, W. Zhu, Citrate route to prepare K-doped Li_2ZrO_3 sorbents with excellent CO_2 capture properties, Chem. Eng. J. 174 (2011) 231–235.
[16] K. Wang, P. Zhao, X. Guo, Y. Li, D. Han, Y. Chao, Enhancement of reactivity in Li_4SiO_4-based sorbents from the nano-sized rice husk ash for high-temperature CO_2 capture, Energy Convers. Manage. 81 (2014) 447–454.
[17] K. Oh-ishi, Y. Matsukura, T. Okumura, Y. Matsunaga, R. Kobayashi, Fundamental research on gas–solid reaction between CO_2 and Li_2CuO_2 linking application for solid CO_2 absorbent, J. Solid State Chem. 211 (2014) 162–169.
[18] I. Alcérreca-Corte, E. Fregoso-Israel, H. Pfeiffer, Absorption on Na_2ZrO_3: a kinetic analysis of the chemisorption and diffusion processes, J. Phys. Chem. C 112 (2008) 6520–6525.
[19] L. Martínez-dlCruz, H. Pfeiffer, Microstructural thermal evolution of the Na_2CO_3 phase produced during a Na_2ZrO_3–CO_2 chemisorption process, J. Phys. Chem. C 116 (2012) 9675–9680.
[20] B. Alcántar-Vázquez, C. Diaz, I.C. Romero-Ibarra, E. Lima, H. Pfeiffer, Structural and CO_2 chemisorption analyses on $Na_2(Zr_{1-x}Al_x)O_3$ solid solutions, J. Phys. Chem. C 117 (2013) 16483–16491.
[21] L.M. Palacios-Romero, E. Lima, H. Pfeiffer, Structural and CO_2 chemisorption study on nonstoichiometric lithium cuprates ($Li_{2+x}CuO_{2+x/2}$), J. Phys. Chem. A 113 (2009) 193–198.
[22] E. Ochoa-Fernández, M. Ronning, T. Grande, D. Chen, Synthesis and CO_2 capture properties of nanocrystalline lithium Zirconate, Chem. Mater. 18 (2006) 6037–6046.
[23] P.R. Díaz-Herrera, M.J. Ramírez-Moreno, H. Pfeiffer, The effects of high-pressure on the chemisorption process of CO_2 on lithium oxosilicate (Li_8SiO_6), Chem. Eng. J. 264 (2015) 10–15.
[24] B. Alcántar-Vázquez, J.F. Gómez-García, G. Tavizon, I.A. Ibarra, C. Diaz, E. Lima, H. Pfeiffer, Structural and ionic conduction analyses of the $Na_2(Zr_{1-x}Al_x)O_{3-x/2}$ solid solution, during the CO_2 chemisorption process, J. Phys. Chem. C 118 (2014) 26212–26218.
[25] T. Nakagaki, Enhanced hydrogen production process from coal integrated with CO_2 separation using dual chemical looping, Energy Process. 4 (2011) 324–332.
[26] M.H. Halabi, M.H.J M. de Croon, J. van der Schaaf, P.D. Cobden, J.C. Schouten, Reactor modeling of sorption-enhanced autothermal reforming of methane. Part I: performance study of hydrotalcite and lithium zirconate-based processes, Chem. Eng. J. 168 (2011) 872–882.
[27] M.H. Halabi, M.H.J.M. de Croon, J. van der Schaaf, P.D. Cobden, J.C. Schouten, Reactor modeling of sorption-enhanced autothermal reforming of methane. Part II: effect of operational parameters, Chem. Eng. J. 168 (2011) 883–888.
[28] J. Liu, L. Dong, W. Guo, T. Liang, W. Lai, CO adsorption and oxidation on N-doped TiO_2 nanoparticles, J. Phys. Chem. C 117 (2013) 13037–13044.
[29] M. Hakamizadeh, S. Afshar, A. Tadjarodi, R. Khajavian, M. Reza-Fadaie, B. Bozorgi, Improving hydrogen production via water splitting over Pt/TiO_2/activated carbon nanocomposite, Int. J. Hydrogen Energy 39 (2014) 7262–7269.
[30] J. Sun, G. Yang, Q. Ma, I. Ooki, A. Taguchi, T. Abe, Q. Xie, Y. Yoneyama, N. Tsubaki, J. Mater. Chem. A 2 (2014) 8637–8643.
[31] R. Soltani, M.A. Rosen, I. Dincer, Assessment of CO_2 capture options from various points in steam methane reforming for hydrogen production, Int. J. Hydrogen Energy 39 (2014) 20266–20275.
[32] A. Alihoseinzadeh, A.A. Khodadadi, Y. Mortazavi, Enhanced catalytic performance of Au/CuO–ZnO catalysts containing low CuO content for preferential oxidation of carbon monoxide in hydrogen-rich streams for PEMFC, Int. J. Hydrogen Energy 39 (2014) 2056–2066.
[33] B. Li, X. Xu, S. Zhang, Synthesis gas production in the combined CO_2 reforming with partial oxidation of methane over Ce-promoted Ni/SiO_2 catalysts, Int. J. Hydrogen Energy 38 (2013) 890–900.
[34] I.G. Osojnik Črniveca, P. Djinović, B. Erjavec, A. Pintar, Effect of synthesis parameters on morphology and activity of bimetallic catalysts in CO_2–CH_4 reforming, Chem. Eng. J. 207–208 (2012) 299–307.
[35] D.J. Suh, C. Kwak, J.H. Kim, S.M. Kwon, T.J. Park, Removal of carbon monoxide from hydrogen-rich fuels by selective low-temperature oxidation over base metal added platinum catalysts, J. Power Sources 142 (2005) 70–74.
[36] W. Han, P. Zhang, Z. Tang, G. Lu, Low temperature CO oxidation over Pd–Ce catalysts supported on ZSM-5 zeolites, Process Saf. Environ. 92 (2014) 822–827.
[37] W. Wang, Y. Jiang, M. Niu, L. Wang, B. Cao, Auto-ignition route to thermoelectric oxide $Na_xCo_2O_4$ powder with high compactibility, Powder Technol. 184 (2008) 25–30.
[38] J.J. Ding, Y.N. Zhou, Q. Sun, X.Q. Yu, X.Q. Yang, Z.W. Fu, Electrochemical properties of P2-phase $Na_{0.74}CoO_2$ compounds as cathode material for rechargeable sodium-ion batteries, Electrochim. Acta 87 (2013) 388–393.
[39] D. Prabhakaran, A.T. Boothroyd, R. Coldea, N.R. Charnley, Crystal growth of Na_xCoO_2 under different atmospheres, J. Cryst. Growth 271 (2004) 74–80.
[40] N. Li, Y. Jiang, G. Li, C. Wang, J. Shi, D. Yu, Self-ignition route to Ag-doped $Na_{1.7}Co_2O_4$ and its thermoelectric properties, J. Alloys Compd. 467 (2009) 444–449.
[41] A.K. Rai, L.T. Anh, J. Gim, V. Mathew, J. Kim, Electrochemical properties of Na_xCoO_2 ($x \sim 0.71$) cathode for rechargeable sodium-ion batteries, Ceram. Int. 40 (2014) 2411–2417.
[42] D. Monti, E. Jónsson, M.R. Palacín, P. Johansson, Ionic liquid based electrolytes for sodium-ion batteries: Na^+ solvation and ionic conductivity, J. Power Sources 245 (2014) 630–636.
[43] C.T. Lin, D.P. Chen, A. Maljuk, P. Lemmens, Sodium cobaltates: crystal growth, structure, thermoelectricity, and superconductivity, J. Cryst. Growth 292 (2006) 422–428.
[44] H. Müller-Buschbaum, On the crystal chemistry of alkali metal oxocobaltates, Z. Anorg. Allg. Chem. 638 (2012) 1932–1957.
[45] M. Miclau, K. Bokinala, N. Miclau, Low-temperature hydrothermal synthesis of the three-layered sodium cobaltite P_3-Na_xCoO_2 ($x \sim 0.60$), Mater. Res. Bull. 54 (2014) 1–5.

[46] S. Lowell, J.E. Shields, M.A. Thomas, Characterization of Porous Solids and Powders: Surface Area, Pore Size and Density, Particle Technology Series, Kluwer Academic Publishers, London, 2004.
[47] T. Ávalos-Rendón, J. Casa-Madrid, H. Pfeiffer, Thermochemical capture of carbon dioxide on lithium aluminates ($LiAlO_2$ and Li_5AlO_4): a new option for the CO_2 absorption, J. Phys. Chem. A. 113 (2009) 6919–6923.
[48] J. Ortiz-Landeros, C. Gomez-Yañez, L.M. Palacios-Romero, E. Lima, H. Pfeiffer, Structural and thermochemical chemisorption of CO_2 on $Li_{4+x}(Si_{1-x}Al_x)O_4$ and $Li_{4-x}(Si_{1-x}V_x)O_4$ solid solutions, J. Phys. Chem. A 116 (2012) 3163–3171.
[49] P. Sánchez-Camacho, I.C. Romero-Ibarra, Y. Duan, H. Pfeiffer, Thermodynamic and kinetic analyses of the CO_2 chemisorption mechanism on Na_2TiO_3: experimental and theoretical evidences, J. Phys. Chem. C 118 (2014) 19822–19832.